

Defect-Induced Fano Resonances in Corrugated Plasmonic Metamaterials

Lin Chen, Ningning Xu, Leena Singh, Tiejun Cui, Ranjan Singh, Yiming Zhu,*
and Weili Zhang*

A novel defect-induced planar meta-atom that supports multiple Fano resonances in a defective corrugated metallic disk (CMD) structure is proposed. Numerical and experimental results reveal that multiple Fano resonances can be excited at terahertz frequencies when the symmetry of the CMD is broken by introducing a small angular defect. These multiple Fano resonances result from mutual coupling between the bright dipolar mode evoked by the edge of the wedge-shaped slice and dark multipole spoof localized surface plasmon modes. Furthermore, the influence of the angle of defect on the Q -factor and the resonance intensity of the quadrupolar resonance peak is investigated. Large values of figure of merit are obtained due to higher Fano resonance intensity and Q -factor. Results from two defective slices in the CMD structure validate the mechanism of the observed phenomenon. The findings of this work would enable a defect-induced Fano resonance platform for biosensing, terahertz domain filtering, and strong light–matter interactions.

scattered states) and quasibound states (resonant states).^[1] Its spectra exhibit the formation of a typical asymmetric line-shaped resonance. The Fano resonance could be easily observed in dielectric and plasmonic systems and has gained tremendous attention due to the potential applications in a broad range of electromagnetic spectrum extending from the microwaves to the optical range.^[2] For example, in metallic hole array structures, the transmission spectrum reveals the Fano resonance, which arises from the interference between a nonresonant and a resonant (associated with surface plasmon excitations at the interfaces of the hole array) scattering process that contributes toward the resonant extraordinary transmission of the incident light.^[3–5] In meta-material systems, asymmetric structures

are often designed to achieve the excitation of the Fano resonance, which is mostly due to the dark trapped modes, induced by the gentle structural symmetry breaking. Symmetry breaking in simple structures has emerged as one of the important findings in the field of plasmonics, as it allows the excitation of the Fano resonances and generates huge enhancement in the electromagnetic field amplitudes.^[6–18] Various asymmetric structures supporting the Fano resonance have been proposed and demonstrated. For instance, asymmetric ring resonators (or split ring resonators) show very sharp Fano resonance at lower frequencies because it can be regarded as the dark mode (only induced in the symmetry broken structure) which has strong interaction with bright modes.^[6,7,11] Other common asymmetric structures, such as asymmetric coupled annular (annular and rectangular hybrid structure),^[15] asymmetric waveguide-cavities system,^[16,17] and asymmetric double bar,^[18] have similar underlying physical principle.

Recently, at microwave and terahertz frequencies, the spoof localized surface plasmons (LSPs) excited at the structured metallic round surface have attracted much attention due to the analogous properties as that of optical LSPs.^[19,20] Multipolar resonances can be observed when spoof LSPs are excited in such structured metasurfaces. At normal incidence, dark multipole modes (spoof LSPs) are suppressed on these metasurfaces (such as corrugated metallic disk (CMD)) due to its symmetry with respect to the exciting field.^[19] Zhen et al. proposed two asymmetric plasmonic CMDs with different sizes in close proximity. The bright dipole mode of small disk couples to the incident light directly, while the dark multiple Fano

1. Introduction

The Fano resonance, discovered by Ugo Fano in 1961, has been described as the interference between continuum of states (the

Prof. L. Chen, Prof. Y. Zhu
Shanghai Key Lab of Modern Optical System
and Engineering Research Center of Optical
Instrument and System (Ministry of Education)
University of Shanghai for Science and Technology
Shanghai 200093, China
E-mail: ymzhu@usst.edu.cn

Prof. L. Chen, Dr. N. Xu, L. Singh, Prof. W. Zhang
School of Electrical and Computer Engineering
Oklahoma State University
Stillwater, OK 74078, USA
E-mail: weili.zhang@okstate.edu

Prof. L. Chen, Prof. T. Cui, Prof. Y. Zhu, Prof. W. Zhang
Terahertz Science Cooperative Innovation Center
Chengdu 610054, China

Prof. T. Cui
State Key Laboratory of Millimeter Waves
Department of Radio Engineering
Southeast University
Nanjing 210096, China

Prof. R. Singh
Centre for Disruptive Photonic Technologies
Division of Physics and Applied Physics
School of Physical and Mathematical Sciences
Nanyang Technological University
Singapore 637371, Singapore



DOI: 10.1002/adom.201600960

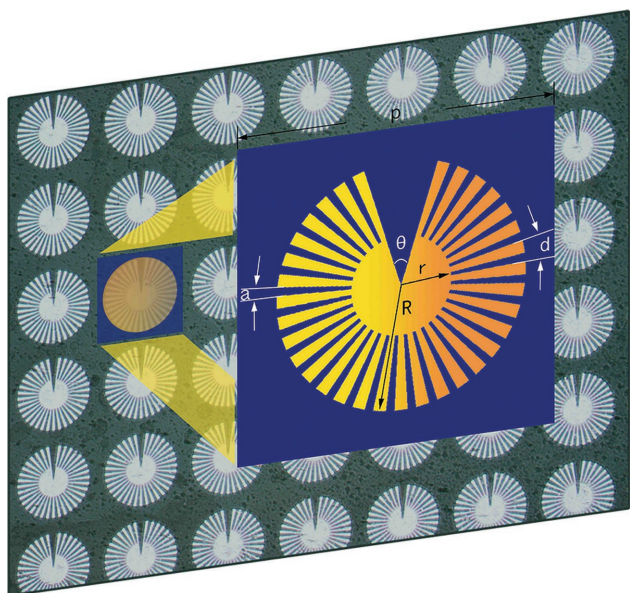


Figure 1. Schematics and microscopic image of the planar defective CMD meta-atom with $r = 60 \mu\text{m}$, $R = 150 \mu\text{m}$, $d = 2\pi R/36$, $a = 0.4d$.

resonances of big disk are excited by near-field coupling mediated by the bright mode.^[21] In our previous work, the dark multiple Fano resonances can also be excited by the bright C-shaped resonator (CSR).^[22] It is important to excite multiple Fano resonances, since it allows an easy and flexible route to match the molecular vibrational resonance with one of the high-quality (Q) Fano resonances by tuning the geometry of the meta-atom unit cell, which not only enables the refractive index sensing by the tightly confined electric field but also reveals highly specific information about molecular specificity.^[13]

In this article, we discuss the design, fabrication and measurement of the flexible asymmetrical corrugated meta-atoms, to provide a new route for exciting multiple Fano resonances in the terahertz range. We found that the multipolar Fano

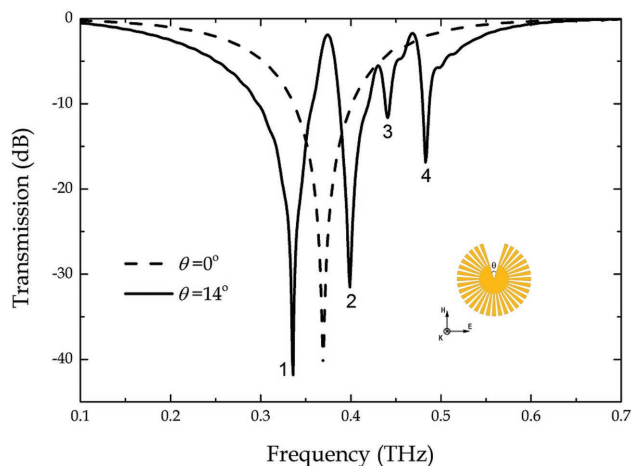


Figure 2. Simulated transmission spectra of symmetric (dash line) and symmetry broken (solid line) CMDs under normal incidence with the angle of defect as 14° . Modes 1, 2, 3, and 4 correspond to dipole, quadrupole, hexapole, and octopole modes, respectively.

resonances (from quadrupole to octopole modes) can be generated when the wedge-shaped slice is cut by a small angle. Fano resonances result from the interference of the bright dipole mode supported by the edge of the missing wedge-shaped slice and dark multipolar modes. Compared to the hybrid metamaterial structures,^[21,22] the present work demonstrates that Fano resonances at terahertz frequencies are easily achievable in individual meta-atoms with simple, planar, contiguous metallic unit cells. The proposed structures could efficiently avoid the

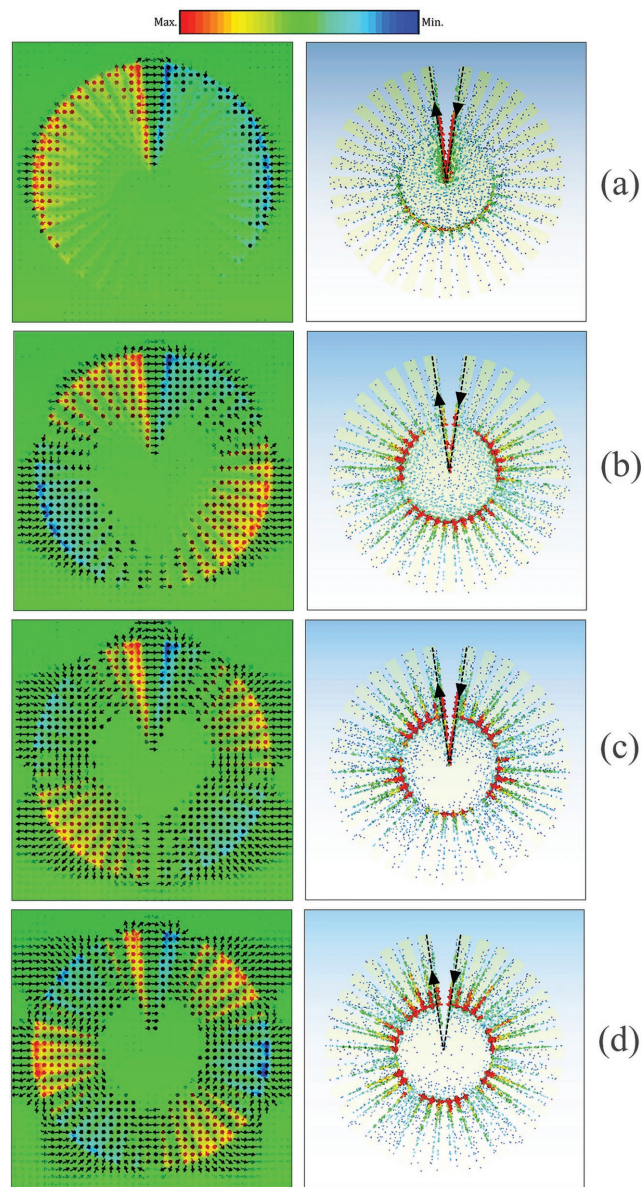


Figure 3. Numerical simulation results of near-electric field and surface current density distributions of the a) dipole, b) quadrupole, c) hexapole, and d) octopole modes. Left: the vertical electric-field distributions of di/quadrupole/hexapole/octopole modes. Arrows represent the electric-field lines, radiating from red (the highest positive intensity) and stopping at dark blue (the lowest negative intensity). Right: surface current density distributions of di/quadrupole/hexapole/octopole modes. Black dashed lines (arrows) indicate the directions of the bright dipole mode which emerges at the edge of the wedge-shaped slice.

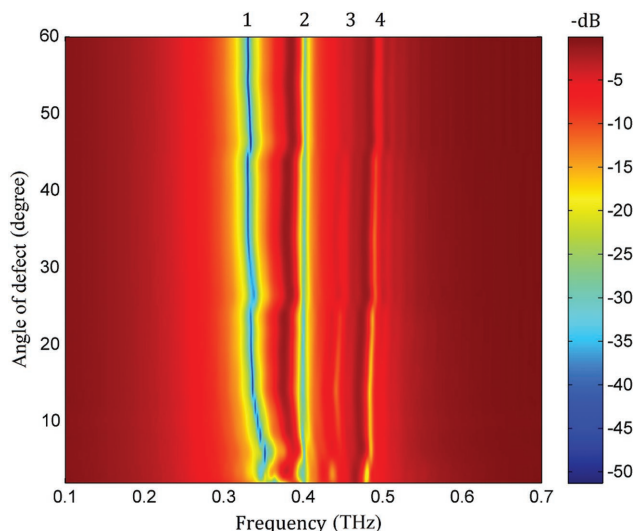


Figure 4. Simulated transmission map for the single defect structure with increasing the angle of defect.

negative interference from other bright elements (small disk in ref. [21] or CSR in ref. [22]), whose resonance frequencies could potentially overlap with dark resonances leading to the distortion or weakening of the Fano resonance (see Supplementary Information in ref. [22]). In addition, the quadrupolar resonance peak shows a high Q feature. The potential of such metamaterials as biochemical sensors has been evaluated with

large values of the Q -factor, resonance intensity, and the figure of merit (FoM) with respect to the angle of defect.

2. Results and Discussion

In **Figure 1**, we schematically illustrated the geometry of the meta-atom with an angular defect of θ . It is composed of the outer radius $R = 150 \mu\text{m}$ and the inner radius $r = 60 \mu\text{m}$ surrounded by periodically radial metallic grooves with the number $N = 36$ and the periodicity $d = 2\pi R/N$. The parameter $a = 0.4d$ is the groove width in the single periodic structure and the thickness of the metallic film (Aluminum, $\sigma_{\text{Al}} = 3.56 \times 10^7 \text{ S m}^{-1}$) $t = 200 \text{ nm}$. The metallic disk is based on a $22 \mu\text{m}$ thick mylar substrate.^[23] The period of the unit cell is $360 \mu\text{m}$. Numerical simulations were performed using CST Microwave Studio to obtain the transmission response of the symmetric ($\theta = 0^\circ$) and defective ($\theta = 14^\circ$) CMD structures, with E -field polarized perpendicular to the defective wedge-shaped slice, as shown in **Figure 2**. A strong dipolar resonance at 0.369 THz was found in the symmetric CMD, which has been verified experimentally in ref. [22]. However, symmetry breaking enables the excitation of multiple dark resonances at normal incidence when the electric field is vertical to the defective slice. Multiple Fano resonances result from the interactions between the dipole bright mode distributed by the edge of the wedge-shaped slice and the multipole dark mode of the remaining corrugated metallic part. In order to clearly understand the origin of such multiple Fano resonances, the electric-field distributions (lines) and surface currents at the resonance

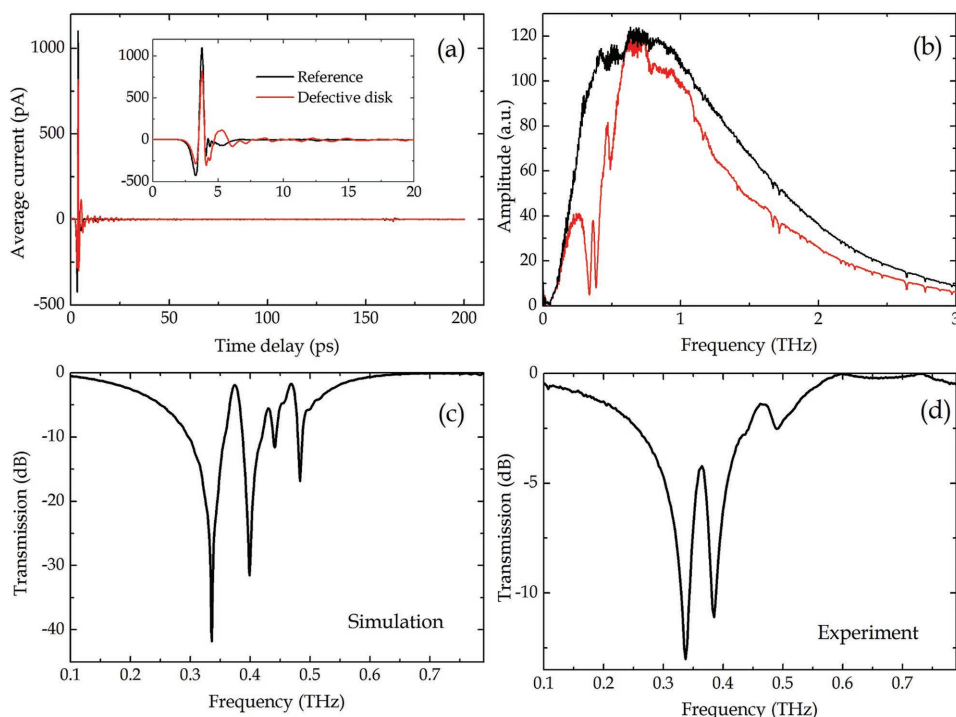


Figure 5. Measured (simulated) time and frequency domain spectra for CMD with one defective slice. a) Terahertz time-domain pulse after transmitting through the blank mylar substrate (reference), and defective CMD sample. b) Fourier transformed frequency-domain transmission spectra of blank mylar substrate, and the defective CMD sample. c) Simulated and d) experimental transmission spectra of the defective CMD with $\theta = 14^\circ$.

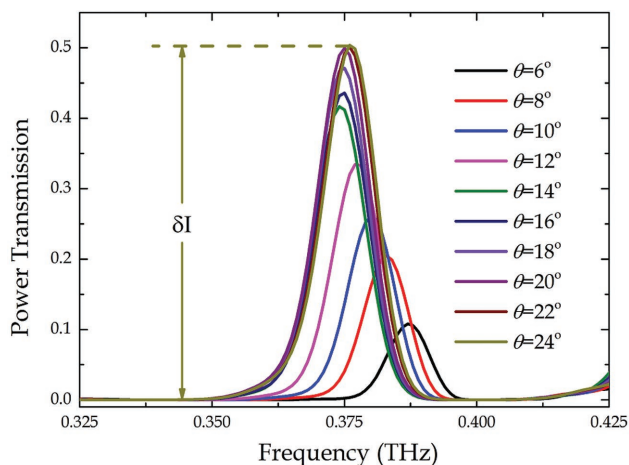


Figure 6. Simulated power transmission spectra comparison among different θ . δI is defined as the power transmission difference from quadrupolar resonance peak to the resonance dip.

dips(1, 0.336 THz; 2, 0.399 THz; 3, 0.441 THz; 4, 0.483 THz) are shown in **Figure 3**(left), where these four modes correspond to 1) dipolar, 1) quadrupolar, 3) hexapolar, and 4) octopolar modes, respectively. **Figure 3**(right) indicates the surface current density at the edge of the wedge-shaped slice which reveals that a bright dipole mode emerges due to the symmetry breaking (black arrows and dash lines). As shown in **Figure 3a**, the electric-field lines (arrows) of both dipolar slice mode and dipolar spoof LSP mode oscillate between positive charge (red) and negative charge (dark blue). Mode 1 (dipole) corresponds to the hybridized bright mode, where the dipolar slice mode and the dipolar spoof LSP mode oscillate in phase, resulting in an increased super-radiative damping. Mode 2 (quadrupole mode) corresponds to the quadrupolar Fano resonance resulting from the coupling of the dipolar slice mode and the quadrupolar spoof LSP mode. It is noteworthy that the bright wedge-shaped dipole mode strongly interacts with the nearby fields of the dipole and the quadrupole modes. Fields which are close to the defect could extend over large area including several sectors that leads to perfect dipolar and quadrupolar patterns as shown in **Figure 3a,b**, respectively. The resonant behaviors for modes 3 and 4 indicate that although two Fano modes result from the interaction between the dipolar slice mode and the multipolar spoof LSP modes (3 and 4 modes), the wedge defect deeply affects the approaching fields of hexa/octopolar modes, as shown in **Figure 3c,d**.

It is intriguing to understand the impact of the varying angle of defect θ on the linewidth and the intensity of the dark Fano resonances. **Figure 4** shows the transmission map with increasing angle of defect from 2° to 60° . First, mode 3(4) becomes weaker due to the fact that the increased defect influences the field distribution 3(4) near the defective slice edge. In other words, the electric fields of hexa/octopole Fano modes become distorted. In contrast, the hybridized dipole mode and the quadrupolar Fano resonances are clearly visible. The quadrupolar transparency window shows discontinuities at special angles (6° , 26° , and 46°). This is due to the discontinuity along the edge of the defect.

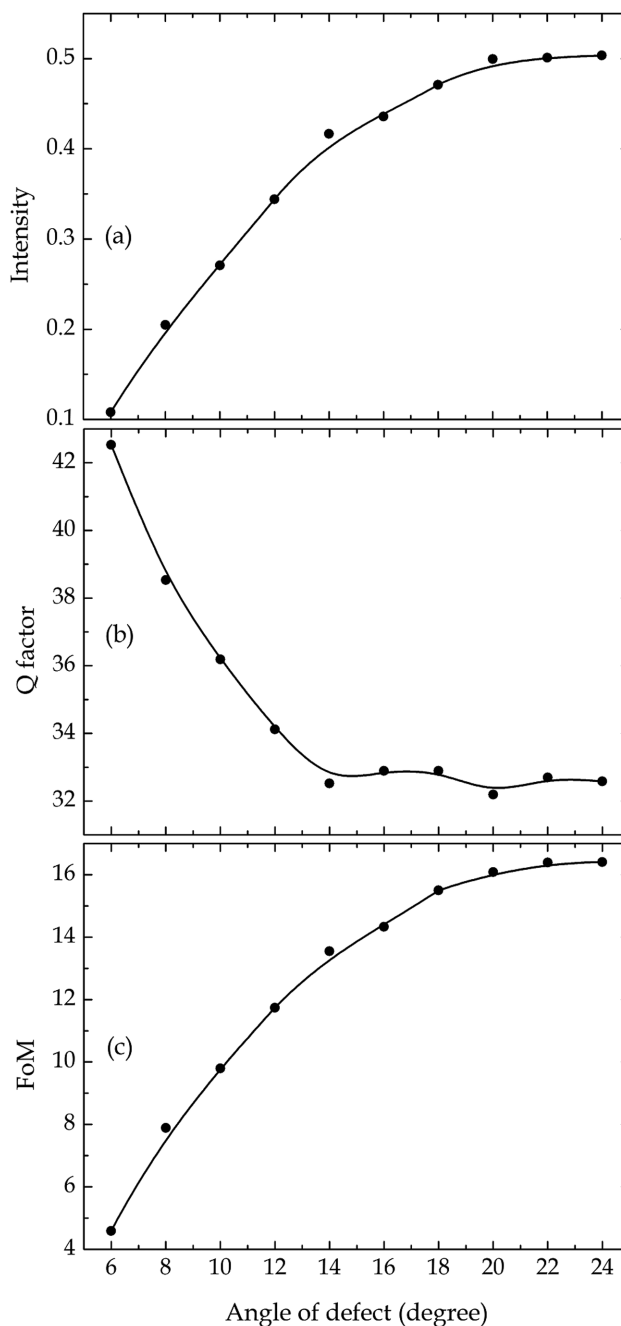


Figure 7. Performance in terms of Figure of merit of the quadrupole resonance peak. a) Resonance strength extracted from simulations. b) Q -factor and c) the FoM versus angle of defect θ . FoM is defined as $\text{FoM} = Q \times \delta I$, where Q is the quality factor of quadrupolar resonance peak and δI is the power transmission difference from Fano resonance peak to the resonance dip.

These multipolar resonances were also observed experimentally. We fabricated the defective CMD using conventional lithography (the microscopic image of the structure has been shown in **Figure 1**). The size of the meta-atom unit cell is $10 \times 10 \text{ nm}^2$. A blank mylar with the identical thickness of the meta-atom substrate was used as a reference. The amplitude transmission spectra of the samples were measured using

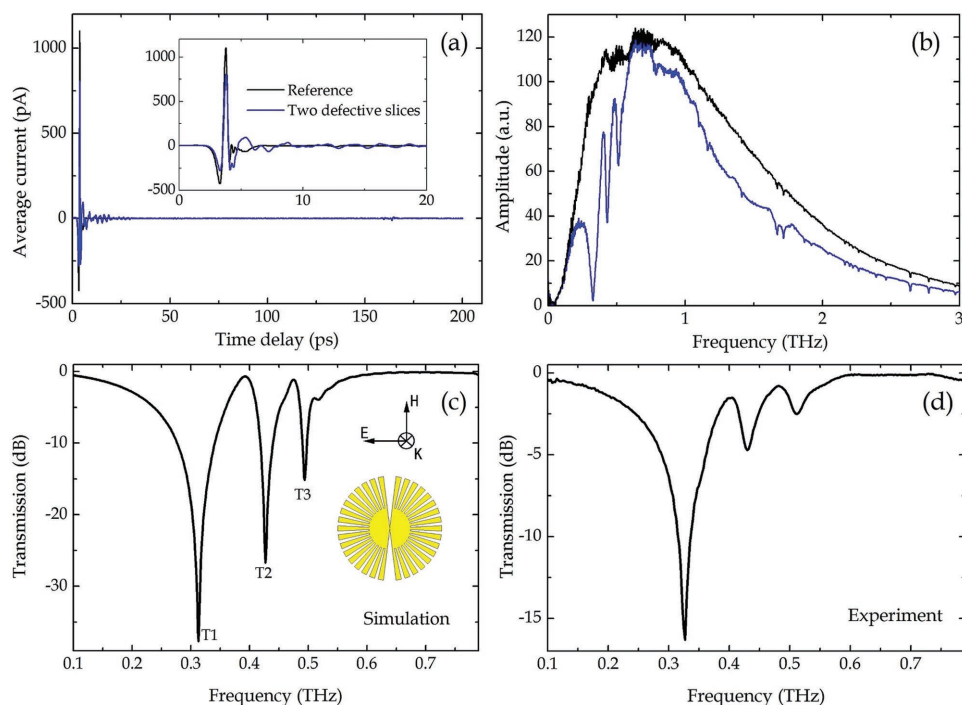


Figure 8. Experimental results and electric-field distributions for CMD with two defective slices. a) Time-domain pulse of reference and sample. b) Frequency-domain transmission spectra of reference and sample. c) Theoretical and d) experimental transmission spectra of sample.

a confocal photoconductive-based 8f terahertz time-domain spectroscopy system.^[24] **Figure 5a** shows the transmitted terahertz time-domain pulse through the blank mylar substrate (reference) and defective CMD sample. The inset of **Figure 5a** shows the zoomed ringing in the terahertz pulses from 0 to 10 ps. The scan time is 200 ps long, which sets the spectral resolution to be 5 GHz.^[16] Corresponding Fourier transformed frequency-domain transmission spectra for the reference (T_{ref} , blank mylar) and sample (T_{dcmd} , $\theta = 14^\circ$) are shown in **Figure 5b**. The simulated normalized transmission NT_{DCMD} (dB) of the single defect structure is calculated (NT_{DCMD} (dB) = $10 \log(T_{\text{dcmd}}/T_{\text{ref}})$) and is illustrated in **Figure 5c**. Strong hybridized dipole mode and quadrupolar resonance associated with the weak hexapolar and octopolar resonances were also observed. The physical mechanism behind this phenomenon is the interaction between the bright wedge-shaped dipole mode and the dark multipolar resonances. Experimental results (**Figure 5d**) also show reasonably good agreement with the simulated transmission spectra. In the simulated and experimental spectra, the hexapole and octopole modes are weak because the defect has a major influence on the fields of the hexa/octopole modes near the defective slice edge. Consequently, these modes cannot be strongly excited and the electric-field distributions do not show the standard hexapole and octopole patterns due to the asymmetry of the defect, as shown in **Figure 3c,d**. The absorption from 1 to 3 THz in **Figure 5b** may be due to the formation of slight concave–convex surface on the flexible mylar substrate of the sample during coating and lithography processes or due to the radiation loss from the metal film.

It is interesting to see that the quadrupolar resonance peak from 0.325 to 0.425 THz shows the Q -value of 30 in

Figure 5b. We plot the simulated power transmission spectra near the quadrupolar resonance peaks at different θ , as shown in **Figure 6**. The transparency window is enhanced with broader linewidth as θ varies from 6° to 14° . To explain this phenomenon, the electric-field distributions at quadrupolar resonance peak for $\theta = 6^\circ$, 14° and 24° are plotted in **Figure S2a–c** in the Supporting Information. According to **Figure S2a** (Supporting Information) ($\theta = 6^\circ$), there exists an obvious discontinuity along the edge of wedge defect. At the position of sawtooth-shaped tip, the electric field is tightly confined, leading to a lower transmission intensity and a narrower linewidth compared to $\theta = 14^\circ$ (**Figure S2b**, Supporting Information). In addition, we attribute the redshift of resonance peak to an increased capacitive coupling between the grating defective part (I) and the inner defective disk part (II) (see **Figure S3** in the Supporting Information). With further increase in θ from 14° to 24° (**Figure S2b,c** Supporting Information), such sawtooth-shaped tip disappears and there is only a minor variation in the resonance linewidth, intensity, and frequency. This fascinating phenomenon enables us to control the intensity and the Q -factor of the transparency window by manipulating the angle of defect. Based on the data extracted from simulations, the dependence of resonance strength on the angle of defect θ is summarized in **Figure 7a**. (Details on the Q -factor calculation can be found in the Supporting Information.) The variation trend of the Q -factor reveals the saturation characteristic of quadrupole intensity with increasing θ . We know that broader linewidths correspond to lower Q -factors.^[7] The Q -factor exhibits the decreasing behavior with the increasing angle of defect θ from 6° to 14° as shown in **Figure 7b**. The quadrupolar resonance intensity is enhanced as the Q factor is lowered. To

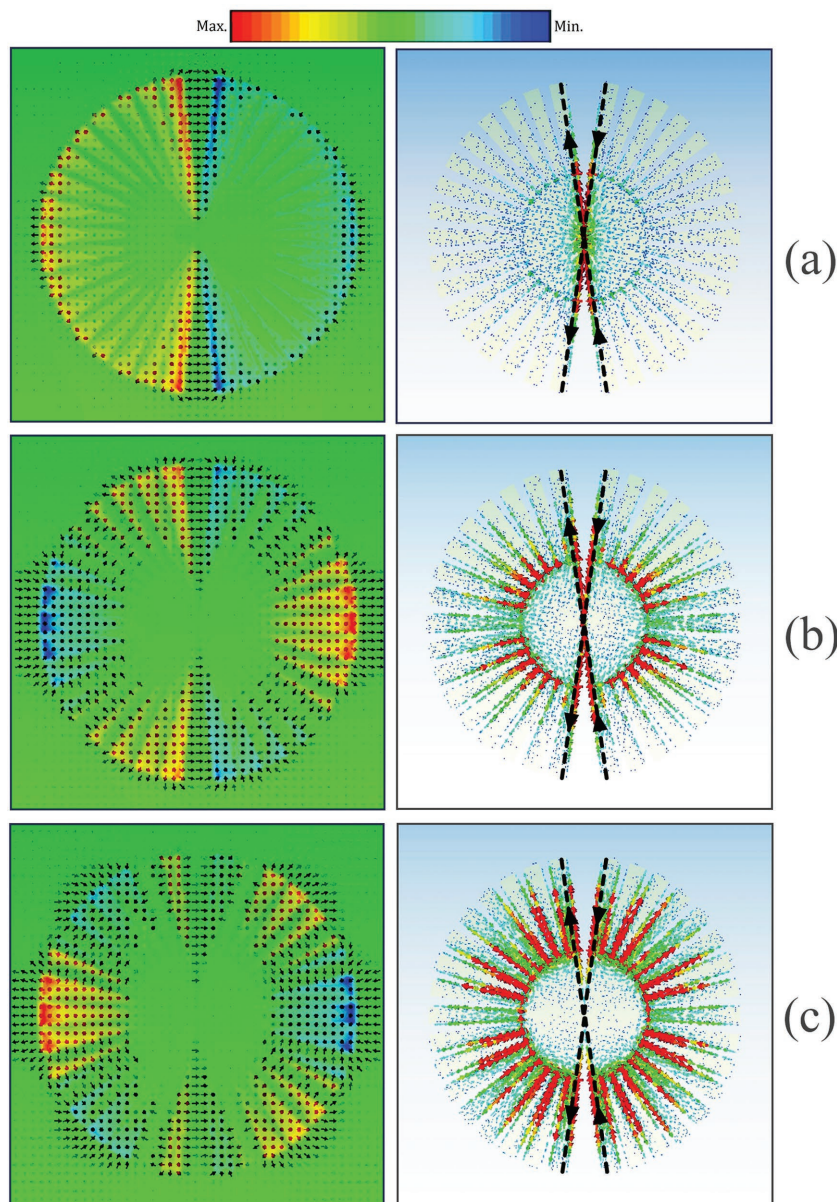


Figure 9. Numerical simulation results of CMD with two defective slices. a) T1 mode, dipole; b) T2 mode, hexapole; c) T3 mode, decapole. Left: the vertical electric-field distributions and the electric-field lines. Right: surface current density distributions. Black dash lines (arrows) indicated the directions of the bright dipole mode which emerges at the top and bottom edges of the wedge-shaped slices.

obtain a value that describes the product of resonance intensity and Q -factor, we define the $\text{FoM} = Q \times \delta I$, where Q is the quality factor and δI is the resonance intensity of the quadrupolar resonance.^[7] This definition of FoM gives clear picture of the resonance Q factor and the intensity. Typically, the Fano excitations are extremely weak due to their weak coupling with the free space. Therefore, it is extremely important to optimize the FoM such that we have a large intensity resonance and narrower linewidths. In addition, it should be noted that both of these parameters, the Q -factor and the resonance intensity, are key parameters for the molecular sensing experiment as the

sensitivity of the structure depends on the linewidth of the Fano resonance and a larger intensity allows easier measurements of the sensing effect. The variation of the FoM is shown in Figure 7c. It can be seen that the best FoM of 16.4 with the quadrupolar intensity of 0.5 and the Q -factor of 32.6 lies at the angle of defect $\theta = 24^\circ$. The FoM for the angle of defect of 14° is 13.6. These FoM values are much higher than the FoM of 6.2 in the asymmetric split ring resonator structures.^[7] Such high FoM performance could be used for ultrasensitive resonant sensing to easily detect thin layers of analyte bonded with the metasurface.^[11,25–27]

To further verify the physical mechanism of multiple Fano resonances based on such defect structure, we fabricated a CMD with two defective slices, where another missing wedge-shaped slice with the same angle of defect is symmetrically cut at the opposite side of CMD. Other parameters are the same as those of the single defect structure in Figure 1. **Figure 8a,b** shows the time and frequency domain spectra of the reference and the sample. Simulated and experimental normalized transmission spectra are illustrated in Figure 8c,d. The inset of Figure 8c depicts the schematic configuration of the proposed structure. Three resonances marked as T1, T2, and T3 can be seen in the simulated and experimental spectra. According to previous discussion, T1 mode represents hybridized dipole resonance, while T2 (T3) mode is multiple Fano resonance. Such higher order dark modes are much more enhanced than those being excited in the single defect structure. This is due to the stronger bright dipole mode excited by the edge of upper and bottom defective wedge-shaped slices. The electric-field distributions (lines) associated with surface current density at resonance frequencies of T1, T2, and T3 give clear schematic indications of the dipole/hexapole/decapole modes and prove this conclusion in the double defect structure, as shown in **Figure 9**. It should be noted that the quadrupole mode cannot be excited in the transmission spectrum

because the phase of its electric field does not match the symmetric feature of the double defect structure. The highest FoM of hexapolar resonance (T2) for the double defect structure is less than that of the single defect structure. Detailed discussion can be found in the Supporting Information.

3. Conclusion

We have proposed an asymmetric CMD structure in the terahertz range which is analogous to the silver–silica–silver

multilayered nanoshells in the visible range.^[28] When an angle of defect is introduced in the CMD, multipolar dark Fano resonances are observed. The electric-field distributions (lines) and surface current density distributions explain the underlying resonance mechanisms. In particular, the quadrupolar transparency peak shows high Q -value and high FoM features. The CMD with two symmetric defective slices was also measured and results verified the physical origin of multiple Fano resonances. These striking characteristics confirm the versatility of the defective CMD structure toward various potential applications. For example, these high Q -value and high FoM Fano features in defect-induced metamaterials could potentially detect the optical properties of thin dielectric films attached onto the meta-atom surface, which is accomplished by tracking the spectral position of the quadrupolar resonance. We can also apply our structure for the detection of analytes, monitoring of chemical reactions, and observation of bacteria pathogens.^[29]

Supporting Information

Supporting Information is available from the Wiley Online Library or from the author.

Acknowledgement

This work was partly supported by the National Program on Key Basic Research Project of China (973 Program, 2014CB339806), Major National Development Project of Scientific Instrument and Equipment (2011YQ15002108, 2012YQ14000504), National Natural Science Foundation of China (61138001, 61205094, 61671302), China Scholarship Council (201508310049), Shanghai Subject Chief Scientist (14XD1403000), and Shanghai Basic Research Key Project (14DZ1206600). L.C., N.X., and W.Z. also acknowledge financial support by the U.S. National Science Foundation (Grand No. ECCS-1232081). We thank Alan Phillips for his language editing contribution.

Received: November 17, 2016

Revised: February 4, 2017

Published online:

[1] U. Fano, *Phys. Rev.* **1961** 124, 1866.

[2] B. Luk'yanchuk, N. I. Zheludev, S. A. Maier, N. J. Halas, P. Nordlander, H. Giessen, C. T. Chong, *Nat. Mater.* **2010**, 9, 707.

- [3] C. Genet, M. P. van Exter, J. P. Woerdman, *Opt. Commun.* **2003**, 225, 331.
- [4] L. Chen, Y. M. Zhu, X. F. Zang, B. Cai, Z. Li, L. Xie, S. L. Zhuang, *Light: Sci. Appl.* **2013**, 2, e60.
- [5] X. Xiao, J. Wu, F. Miyamaru, M. Zhang, S. Li, M. W. Takeda, W. Wen, P. Sheng, *Appl. Phys. Lett.* **2011**, 98, 011911.
- [6] R. Singh, I. A. I. Al-Naib, Y. Yang, D. R. Chowdhury, W. Cao, C. Rockstuhl, T. Ozaki, R. Morandotti, W. Zhang, *Appl. Phys. Lett.* **2011**, 99, 201107.
- [7] L. Cong, M. Manjappa, N. Xu, I. Al-Naib, W. Zhang, R. Singh, *Adv. Opt. Mater.* **2015**, 3, 1537.
- [8] F. Hao, Y. Sonnefraud, P. V. Dorpe, S. A. Maier, N. J. Halas, P. Nordlander, *Nano Lett.* **2008**, 8, 3983.
- [9] V. A. Fedotov, M. Rose, S. L. Prosvirnin, N. Papasimakis, N. I. Zheludev, *Phys. Rev. Lett.* **2007**, 99, 147401.
- [10] M. Kang, H.-X. Cui, Y. Li, B. Gu, J. Chen, H.-T. Wang, *J. Appl. Phys.* **2011**, 109, 014901.
- [11] R. Singh, W. Cao, I. Al-Naib, L. Cong, W. Withayachumnankul, W. Zhang, *Appl. Phys. Lett.* **2014**, 105, 171101.
- [12] I. A. I. Al-Naib, C. Jansen, M. Koch, *Appl. Phys. Lett.* **2008**, 93, 083507.
- [13] C. Wu, A. B. Khanikaev, R. Adato, N. Arju, A. A. Yanik, H. Altug, G. Shvets, *Nat. Mater.* **2011**, 11, 69.
- [14] Z. Fang, J. Cai, Z. Yan, P. Nordlander, N. J. Halas, X. Zhu, *Nano Lett.* **2011**, 11, 4475.
- [15] G. Dayal, X. Y. Chin, C. Soci, R. Singh, *Adv. Opt. Mater.* **2016**, 4, 1295.
- [16] L. Chen, C. M. Gao, J. M. Xu, X. F. Zang, B. Cai, Y. M. Zhu, *Opt. Lett.* **2013**, 38, 1379.
- [17] S. Fan, *Appl. Phys. Lett.* **2002**, 80, 908.
- [18] F. Zhang, X. Huang, Q. Zhao, L. Chen, Y. Wang, Q. Li, X. He, C. Li, K. Chen, *Appl. Phys. Lett.* **2014**, 105, 172901.
- [19] A. Pors, E. Moreno, L. Martin-Moreno, J. B. Pendry, F. J. Garcia-Vidal, *Phys. Rev. Lett.* **2012**, 108, 223905.
- [20] X. Shen, T. J. Cui, *Laser Photonics Rev.* **2014**, 8, 137.
- [21] Z. Liao, B. C. Pan, X. Shen, T. J. Cui, *Opt. Express* **2014**, 22, 15710.
- [22] L. Chen, Y. M. Wei, X. F. Zang, Y. M. Zhu, S. L. Zhuang, *Sci. Rep.* **2016**, 6, 22027.
- [23] J. Gu, J. Han, X. Lu, R. Singh, Z. Tian, Q. Xing, W. Zhang, *Opt. Express* **2009**, 17, 20307.
- [24] D. Grischkowsky, S. Keiding, M. Exter, Ch. Fattinger, *J. Opt. Soc. Am. B* **1990**, 7, 2006.
- [25] J. F. O'Hara, W. Withayachumnankul, I. Al-Naib, *J. Infrared, Millimeter, Terahertz Waves* **2012**, 33, 245.
- [26] M. Manjappa, Y. K. Srivastava, L. Cong, I. Al-Naib, R. Singh, *Adv. Mater.* **2017**, 29, 1603355.
- [27] Y. K. Srivastava, M. Manjappa, H. N. S. Krishnamoorthy, R. Singh, *Adv. Opt. Mater.* **2016**, 4, 1875.
- [28] J. F. Ho, B. Luk'yanchuk, J. B. Zhang, *Proc. SPIE* **2010**, 7730, 77301S.
- [29] E. Pickwell, V. P. Wallace, *J. Phys. D: Appl. Phys.* **2006**, 39, R301.